Chemical Science

ROYAL SOCIETY OF CHEMISTRY

EDGE ARTICLE

View Article Online
View Journal | View Issue

Cite this: *Chem. Sci.*, 2021, **12**, 13151

All publication charges for this article have been paid for by the Royal Society of Chemistry

Received 6th May 2021
Accepted 8th September 2021

DOI: 10.1039/d1sc02518j

rsc.li/chemical-science

Design of an electrochemiluminescence detection system through the regulation of charge density in a microchannel†

Yanling Huang,[a] Yilei Lu,[a] Xiaobin Huang,[a] Jian Wang,[a] Bin Qiu,[a] Fang Luo*[ab] and Zhenyu Lin*[a]

Rare electrochemiluminescence (ECL) sensors have been developed based on the direct regulation of ionic current because it is difficult to establish a relationship between ionic current and ECL reporting. Ionic current can be adjusted by the effective radius and charge density of a functionalized microchannel and is frequently adopted to develop electrical sensors. Here, we show a novel ECL sensing platform that combines the microchannel-based electrical sensing technology with an ECL reporting system for the first time. The target regulated the effective radius and charge density of a microchannel which in turn adjusted the ionic transport in it and finally caused the change of ECL reporting of a tris(1,10-phenanthroline)ruthenium(II)/tripropylamine system. The developed system has already been applied to detect aflatoxin B1 for demonstration. This configuration separated the target sensing and reporting reactions to achieve direct regulation of ECL reporting by ionic current and expanded the application of the ECL detection technology to microanalysis.

Introduction

Electrochemiluminescence (ECL) is a combination of electrochemical and chemiluminescence reactions that occur at/near the electrode surface,[1,2] and has been extensively used in many fields owing to the characteristics of low background signal, high sensitivity and ease of use with low cost instruments.[3] In traditional ECL detection systems, electroactive materials are oxidized or reduced at the electrode surface under appropriate potential to form active species that are relaxed to the ground state and emit light.[4] The ECL intensity was regulated by the concentrations of the luminophore and co-reactant, the luminous efficiency of the luminophore, the parameters of instruments such as electrode materials and areas, cell geometries, applied potentials and so on.[5–8] Bipolar electrode (BPE) ECL detection systems have attracted extensive attention because the analytes need not participate in the ECL reactions directly.[9,10] Charge balance permitted the ECL reaction occurring at the anode of the BPE to relate to the reduction reaction occurring at the cathode.[11,12] Therefore, the ECL intensity was not only dependent on the concentrations of the luminophore and co-reactant, the luminous efficiency of the luminophore and instrumental parameters, but also related to the ionic current passing through the system. Besides, early studies also indicated that it had a direct relationship with ionic current passing through the working electrode.[10,13] However, few ECL detection systems have been designed based on this relationship until now.

Artificial channel structures (nanochannels or microchannels) have been widely studied in protein recognition[14,15] and molecule analysis[16,17] due to their strong chemical stability, controllable channel shape, and tailorable surface chemistry.[18–21] In addition, they can also act as connecting devices between electrolyte-containing chambers. The ions/molecules can move through the channels or react with the recognition units that are attached to the inner surface of the channels. The target recognition reactions adjusted the effective radius and the charge density along the channel structures which in turn altered the ionic transport inside them.[22–30] In early reports, artificial channels were combined with ECL detection to design new ECL detection systems, where nanochannel structures acted as the gate and attached to the surface of the working electrode. The amount of electroactive material entering the nanochannels depended on the effective radius and the electrostatic interactions between the electroactive materials and the functionalized nanochannels.[31–33] However, artificial channels that can regulate the ion current and directly adjust the

[a]*Ministry of Education Key Laboratory for Analytical Science of Food Safety and Biology, Fujian Provincial Key Laboratory of Analysis and Detection for Food Safety, College of Chemistry, Fuzhou University, Fuzhou, Fujian, 350116, China. E-mail: zylin@fzu.edu.cn*

[b]*College of Biological Science and Engineering, Fuzhou University, Fuzhou, Fujian, 350116, China. E-mail: luofang@fzu.edu.cn*

† Electronic supplementary information (ESI) available: Generation of platform current; verification of the generation of the EOF; the effect of the EOF on ion distribution; the effect of half cone angle on the EOF; optimization of the experimental parameters; and the application of the proposed microchannel-based ECL sensor. See DOI: 10.1039/d1sc02518j

redox reactions of the electroactive substances on the working electrode surface have never been applied in the design of ECL detection systems.

In this work, an artificial microchannel-based ECL detection system was developed based on ionic current being directly regulated by artificial channels, and then the ECL intensity of the reporting system being further affected. A tris(1,10-phenanthroline)ruthenium(II) ($Ru(phen)_3^{2+}$)/tripropylamine (TPrA) system was used in our previous work.[34] It possessed similar performance to the commonly used tris(2,2′-bipyridine)ruthenium(II) $Ru(bpy)_3^{2+}$/TPrA and $Ru(bpy)_3^{2+}$/2-(dibutylamino) ethanol system[35,36] and therefore was adopted as the model ECL reporting system in the current work. A glassy carbon electrode (GCE) and a platinum (Pt) electrode acted as the driving electrodes and were linked to a microchannel. A functionalized microchannel was selected as the target recognition element to regulate ionic current. When a potential was applied between the GCE and Pt electrode, the correlation between ionic currents staying on the GCE and passing through microchannels was connected *via* charge balance. In consequence, the ECL intensity of the system showed a relationship with the ionic current passing through the microchannel. As the ionic current depended on the effective radius and charge density of the microchannel, this approach enabled the regulation of the ECL intensity through the regulation of the ionic current passing through the microchannel.

Results and discussion

Design of a microchannel-based ECL sensing platform

Scheme 1 shows the system of the proposed microchannel-based ECL sensing platform. This design was based on a standard electrochemical cell in which three electrodes were connected to an electrochemical workstation. There was a voltage difference between the GCE and Pt electrode that were separately situated in two reservoirs which were linked by a microchannel (Scheme 1a). The potential of the GCE corresponded to that of the Ag/AgCl electrode (3 M KCl). The microchannel had high resistance, so most of the E_{total} (the total potential applied by the workstation) dropped at the terminal of the microchannel, and the partial potential applied on the GCE (*vs.* Ag/AgCl) was lower than the setting potential. And the electrochemical workstation automatically adjusted this lowness to equality which, however, could not be achieved. When the applied potential between the GCE and Pt electrode reached a maximum value (14 V in this system), the platform current was observed (Fig. S1, ESI†). For the target sensing reaction, the target recognition reaction altered the effective radius and charge density of the microchannel and hence regulated the ionic current passing through the microchannel. The correlation between ionic currents staying on the GCE and passing through the microchannel was connected *via* charge balance; therefore, the oxidation reaction of the luminophore on the GCE surface was regulated by the ionic current across the microchannel. This configuration separated the sensing and reporting reactions, thus achieving the direct regulation of ECL reporting by ionic current.

Chemical covalent modifications were used to provide the microchannel with the function of a recognition element, and then the target was combined with the recognition element to regulate the effective radius and charge density of the microchannel (Scheme 1b). When the size or dimensionality of the uncharged target was comparable with the radius of microchannel, the effective radius would decrease after the uncharged target attached to the inner surface of the microchannel. The ionic transport was blocked in the microchannel with smaller effective radius under the driving force of electrophoresis (EP), thus resulting in a decrease in ionic current and ECL intensity (Scheme 1c). When the size or dimensionality of the charged target was negligible compared with the radius of the microchannel, the charge density would regulate the ionic current (Scheme 1d). Negatively charged recognition units were coated on the interior of the microchannel, and mobile cations were attracted to the negatively charged surface and formed an electrical double layer (EDL). These cations dragged the fluid toward the cathode to form an electroosmotic flow (EOF) which contradicted with the EP, prevailing in ion transport, and increased with the increase of the negative charge density, resulting in the depletion of movable ions at the tip of the microchannel with higher negative charge density. Besides, the EOF induced ion depletion at the tip of the microchannel, thus causing a decrease in ionic current and ECL intensity. Therefore, the microchannel-based ECL sensing platform can be used to detect targets with the ability of regulating the effective radius and charge density of the microchannel.

Verification of the feasibility of the microchannel-based ECL sensing platform

To verify our above hypothesis, the influences of effective radius and charge density on ionic current and ECL intensity were studied. Microchannels with different diameters were prepared to simulate the effective radius regulation process of the target. Conical glass microchannels with tip diameters of 1–60 μm were fabricated. The ionic current increased with the increase of microchannel diameter due to the low ionic resistivity of ionic transport (Fig. 1a). Fig. 1b shows the ECL–potential curves and the inset shows the ECL intensity of bare microchannels with different diameters. As it displays, the ECL intensity increased at first and then tended to be steady with the increase of microchannel diameter. This phenomenon appeared probably because the confinement effect from the microchannel was decreased in the microchannel with larger diameter. Fig. 1c shows the relationship between ECL intensity and platform current, that is, the ECL intensity increased with the increase of ionic current, and an ECL platform was observed in the microchannel with larger diameter. On the basis of these results, microchannel-based ECL biosensors can be designed for target sensing when the target size is comparable with the diameter of the microchannel.

DNA is a negatively charged nanoscale molecule in dimensionality owing to its rich phosphoric acid skeleton. Compared to the microchannel on the microscale, the dimensionality of DNA is negligible. Therefore, the effect of negative charge

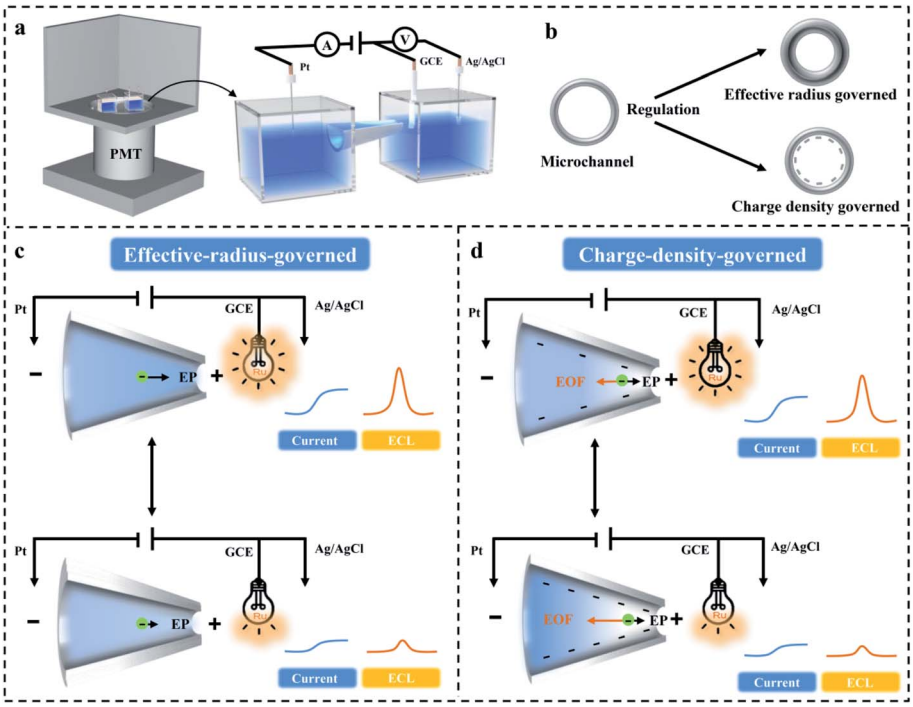

Scheme 1 The design of the microchannel-based ECL sensing platform. (a) The instrumentation for the microchannel-based ECL sensor platform. (b) The effective radius and charge density of the microchannel were regulated by surface modification. The mechanisms of (c) effective radius and (d) charge density regulation of ionic current and ECL reporting.

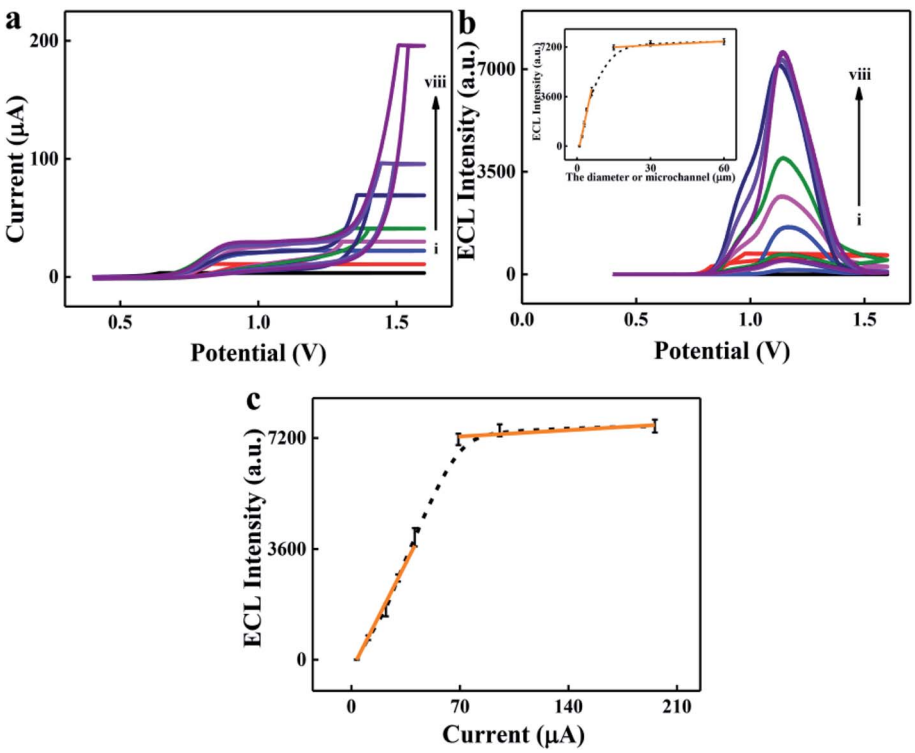

Fig. 1 The effect of effective diameter of the microchannel on ionic current and ECL intensity; (a) *I*–*V* curves, (b) ECL–potential curves at different diameters of the microchannels and the inset shows the ECL intensity of bare microchannels with different diameters. (c) The relationship between ECL intensity and platform current. The diameters of bare microchannels from (i) to (viii) were 1, 2, 3, 4, 6, 15, 30 and 60 μm. The bulk solution contained Tris (10 mM), KCl (0.6 M), $Ru(phen)_3^{2+}$ (5 μM) and TPrA (13 mM). The pH of the solution was 8.0. The three-electrode system contained a GCE (3 mm diameter), a Pt electrode (0.5 mm diameter) and an Ag/AgCl electrode (3 M KCl) as the working electrode, counter electrode and reference electrode, respectively.

density on ionic current and ECL reporting was studied using a DNA functionalized microchannel as an example. Ionic current and ECL intensity increased with the decrease of negative charge density of the microchannel with 3 μm diameter (Fig. 2a–c). The potential of the initial ECL emission was about 0.8 V, while the maximum ECL emission potential occurred at the potential where the platform current disappeared (Fig. 2c and the description is shown in S3, ESI†). After that, the effect of negative charge density on ionic current was studied *via* synchronous electrochemical and optical assays; neutral, negatively charged and positively charged optical probes were depleted at the tip of a negatively charged microchannel (Fig. S2, ESI†). These results demonstrated that an EOF generates from the tip to base in the negatively charged microchannel. The EOF caused the depletion of cations and anions at the tip of the microchannel. The ionic current depends on the ionic concentration at the tip of the microchannel, and the charge balance permitted the ECL output to correlate to the ionic current passing through the microchannel.[37,38] Therefore, the ionic current and ECL intensity decreased with the increase of negative charge density of the inner surface of the microchannel.

However, the change of the negative charge density caused by DNA cannot affect the ionic current and ECL intensity in the microchannel with 6 μm diameter (Fig. 2d–f). The ECL intensity as a function of potential in our work was similar to that in traditional ECL systems; the potential values of initial and maximum ECL emission were about 0.8 V and 1.2 V, respectively. The main reason was that the charge in the EDL of the microchannel with relatively large diameter cannot affect the ionic transport in the microchannel.[25] The half cone angle also affects the ionic transport in the microchannel and its optimized value was 5° (Fig. S3, ESI†). Therefore, a microchannel with a diameter of 3 μm and a half cone angle of 5° was selected in the following study. Given these outcomes, a charge density regulated microchannel-based ECL sensor can be designed for target sensing.

Application of the microchannel-based ECL sensing platform

To confirm the application, a "negative charge density decrease" microchannel-based ECL sensor was developed (Fig. 3a). Aflatoxin B1 (AFB1) was used as a model target to regulate the negative charge density of the microchannel. The capture DNA (cDNA)/aptamer complex was first attached to the inner surface of the microchannel. Then in the presence of the target, the AFB1 aptamer dissociated from it due to the strong combination between AFB1 and the AFB1 aptamer (Fig. S5a, ESI†). The release of the AFB1 aptamer caused the decrease of negative charge density in the inner surface of the microchannel (Fig. 3b and S5b, ESI†). The EOF from the tip to base dropped with the decrease of negative charge density of the microchannel. As a result, the microchannel converted into a high conductance state.

The experimental conditions were optimized, and the details are shown in S6, ESI.† The performance of the proposed microchannel-based ECL sensor was tested under the optimized experimental conditions (Fig. S4, ESI†). ECL intensity increased with the increase in AFB1 concentration ranging from

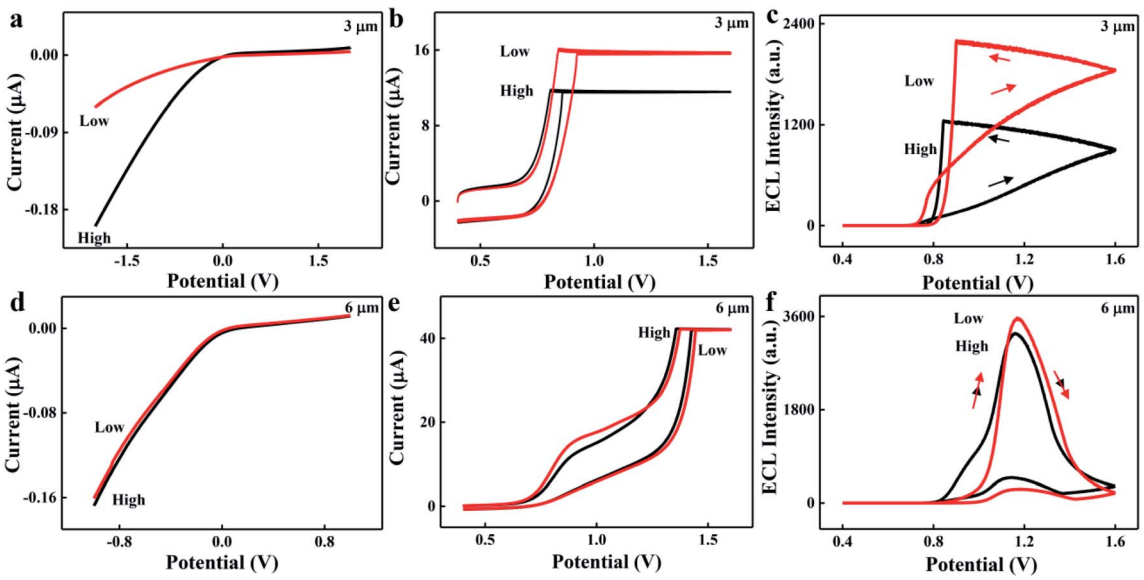

Fig. 2 (a) The effect of negative charge density on ionic current in an ionic current rectification system of functionalized microchannels with 3 μm diameter. (b) *I*–*V* curves and (c) ECL–potential curves of functionalized microchannels (3 μm diameter) with different negative charge densities. (d) The effect of negative charge density on ionic current in an ionic current rectification system of functionalized microchannels with 6 μm diameter. (e) *I*–*V* curves and (f) ECL–potential curves of functionalized microchannels (6 μm diameter) with different negative charge densities. In the ionic current rectification system, functionalized microchannels were immersed in KCl (10 mM) solution and a pair of Ag/AgCl electrodes acted as driving electrodes. In the microchannel-based ECL detection system, functionalized microchannels were immersed in bulk solution containing Tris (10 mM), KCl (0.6 M), $Ru(phen)_3^{2+}$ (5 μM) and TPrA (13 mM). The pH of the solution was 8.0, and the three-electrode system contained a GCE (3 mm diameter), a Pt electrode (0.5 mm diameter) and an Ag/AgCl electrode (3 M KCl).

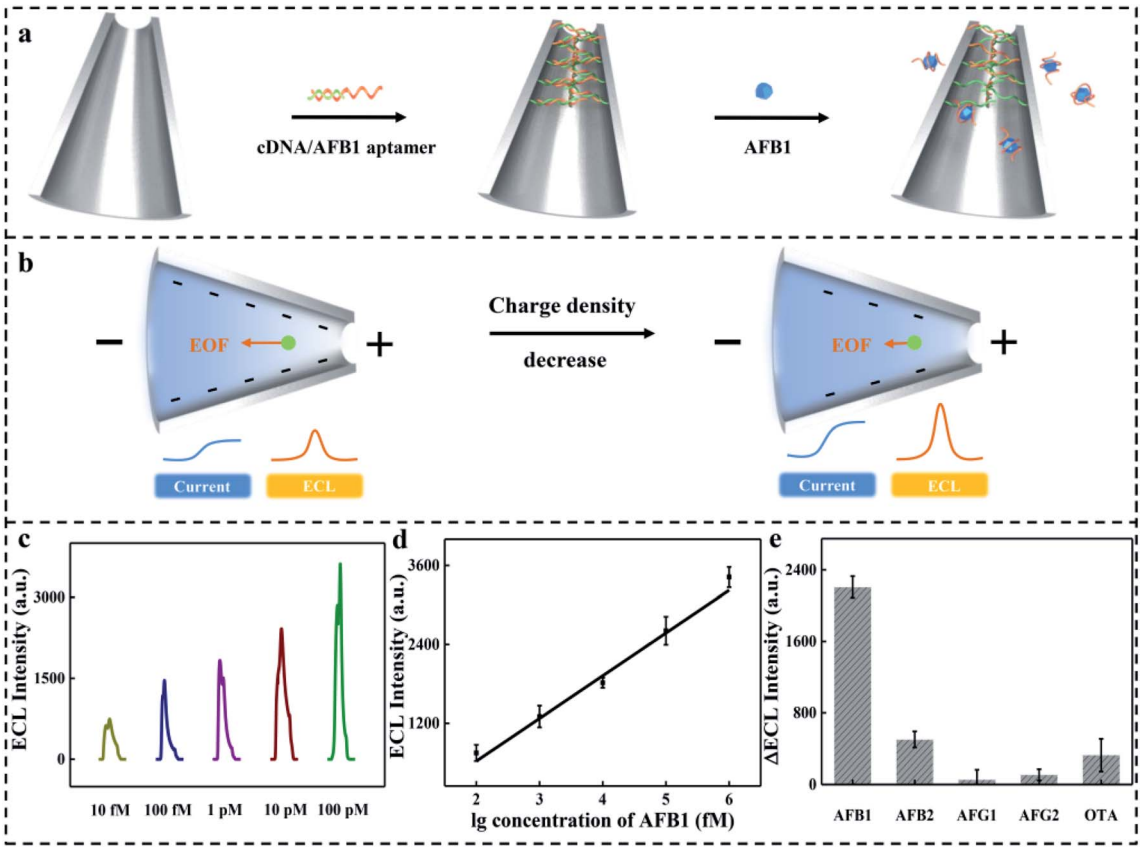

Fig. 3 (a) The scheme of the "negative charge density decrease" microchannel-based ECL sensor for AFB1 detection. (b) The mechanism of the proposed microchannel-based ECL sensor. (c) ECL intensity and (d) calibration curve of the microchannel-based ECL sensor obtained by immersing the cDNA/aptamer functionalized microchannel in AFB1 solution with different concentrations (10 fM, 100 fM, 1 pM, 10 pM and 100 pM). (e) The selectivity of the proposed microchannel-based ECL sensor. The concentrations of AFB1 and potential AFB1 interferents were 10 pM and 100 pM, respectively. The bulk solution contained Tris (10 mM), KCl (0.6 M), $Ru(phen)_3^{2+}$ (5 μM) and TPrA (13 mM). The pH of the solution was 8.0. The three-electrode system contained a GCE (3 mm diameter), a Pt electrode (0.5 mm diameter) and an Ag/AgCl electrode (3 M KCl).

10 fM to 100 pM (Fig. 3c). There was a good linear relationship between I_{ECL} (represents ECL intensity) and lg C_{AFB1} (represents logarithmic concentration of AFB1) (Fig. 3d). The equation of the standard curve is expressed as follows:

$$I_{ECL} = 650 \lg C_{AFB1} - 677,\ R^2 = 0.97$$

where R represents the correlation coefficient. The limit of detection (LOD) was estimated to be 3.3 fM (S/N = 3). When the ionic current in the ionic current rectification system was employed as the readout, the rectification ratio (RR, which represents the ratio of the ionic current at −2 V and that at 2 V) was inversely proportional to lg C_{AFB1} in the range from 10 pM to 100 nM (Fig. S5c and d, ESI†). The equation of the standard curve is expressed as follows:

$$RR = -4.58 \lg C_{AFB1} - 41.5,\ R^2 = 0.98.$$

The LOD was estimated to be 3.3 pM (S/N = 3). The selectivity was also further studied because it is also an important parameter for sensors. As shown in Fig. 3e, the target (10 pM) was replaced with other interfering substances (100 pM) such as aflatoxin B2 (AFB2), aflatoxin G1 (AFG1), aflatoxin G2 (AFG2), and ochratoxin A (OTA) present in contaminated agricultural products. Little signal was observed for interference substances, while obvious signal was observed for the target, confirming that the aptamer-functionalized microchannel-based ECL sensor had a good selectivity for AFB1 detection.

Peanuts were selected as the representative sample to confirm its potential application in real samples. The concentration of AFB1 in real samples was detected after pre-treatment (S7, ESI†). The recovery rate of AFB1 detection was in the range of 96.21 to 105.6% and the relative standard deviation (RSD) ranged from 2.37 to 4.52%. To further confirm the analytical applicability of the proposed method in real samples, high-performance liquid chromatography-tandem mass spectrometry (HPLC-MS/MS) assays were performed, and the results indicated that the proposed microchannel-based ECL sensor can be used for AFB1 detection in real samples (Table S1, ESI†).

Conclusions

In summary, we for the first time combined microchannel-based target sensing reactions with ECL reporting reactions,

where the target sensing reactions occurred at the microchannel and reported the target's presence *via* ECL emission at working electrodes. This configuration separated sensing and reporting reactions to achieve direct regulation of ECL reporting by ionic current. In addition, the proposed microchannel-based ECL sensor showed excellent performance for the quantification of the target, which could regulate the effective radius and charge density of the microchannel, thus expanding the application of the ECL detection technology to microanalysis.

Experimental

Fabrication of the microchannel

A freshly prepared piranha solution (volume ratio was 3 : 7, 98% H_2SO_4/30% H_2O_2) was used to remove contaminating residues on quartz glass capillaries which were then pulled using a micropipette puller. The programs with the following settings were used: heat 500, filament 4, velocity 45, delay 200, pulling 0; heat 450, filament 4, velocity 30, delay 200, pulling 30.

Functionalization of the microchannel

Carboxyl-modified microchannels were fabricated according to a previous report.[39] The tips of the microchannels were backfilled with freshly prepared 3-aminopropyltriethoxysilane (APTES, 10%, in ethanol) for 1 h, followed by washing with ethanol to obtain amino-modified microchannels that were immersed in succinic anhydride (SA, 0.01 g mL^{-1}, in dimethyl sulfoxide) for 4 h afterwards. Carboxyl-modified microchannels were obtained by washing the prepared microchannels with ethanol. cDNA-functionalized microchannels were prepared by immersing carboxyl-functionalized microchannels in PBS buffer (10 mM, pH = 7.0) containing 1-ethyl-3-(3′-dimethylaminopropyl) carbodiimide (2 mg mL^{-1}, EDC), *N*-hydroxy succinimide (1 mg mL^{-1}, NHS) and DNA (1 μM) for 10 h, and amine-modified cDNA was attached to the carboxyl-modified microchannel by the EDC/NHS coupling reaction. And then cDNA was combined with the AFB1 aptamer to form a cDNA/aptamer complex, which transformed into the cDNA/aptamer complex-functionalized microchannel after being washed with Tris–HCl buffer.

Microchannel-based ECL sensor for AFB1 detection

The cDNA/aptamer complex-functionalized microchannels were first immersed in AFB1 solutions with different concentrations at room temperature for 2 h and then rinsed with Tris–HCl buffer to remove redundant AFB1 and the released AFB1/aptamer complex. Afterwards, the obtained target-functionalized microchannels were mounted in the developed ECL system to perform ECL detection.

Measurement of the *I–V* curve and ECL intensity

In the ionic current rectification system, one Ag/AgCl electrode (0.5 mm diameter) was inserted into the microchannel and served as the working electrode, and another Ag/AgCl electrode (0.5 mm diameter) was placed in an external electrolyte bath and acted as the auxiliary/reference electrode. The composition of the solution inside the microchannel was the same as that of the bulk solution with KCl (10 mM). The ionic current rectification was recorded by scanning the voltage from −2.0 to 2.0 V at a scan rate of 50 mV s^{-1}. In the ECL detection system, a three-electrode system containing a GCE (3 mm diameter), a Pt electrode (0.5 mm in diameter), and an Ag/AgCl electrode (3 M KCl) was used for further study. The GCE and Pt electrode were separated by a microchannel. Cyclic potential scan was conducted to excite ECL emission from the electrochemical workstation, and the ECL emission was collected by the luminescence analyser. The ionic current and ECL intensity were recorded by scanning the voltage from 0.4 to 1.6 V. The voltage of the photomultiplier tube (PMT) was regulated in −600 V.

Data availability

Relevant data are presented in the manuscript and ESI.†

Author contributions

Y. L. H. and Z. Y. L. conceived and designed the study; Y. L. H., X. B. H. and Y. L. L. conducted the experiments; Y. L. H., J. W., F. L., B. Q. and Z. Y. L. analysed the data; Y. L. H., F. L. and Z. Y. L. wrote the paper.

Conflicts of interest

There are no conflicts to declare.

Acknowledgements

This project was supported by the National Natural Science Foundation of China (21974020) and the United Fujian Provincial Health and Education Project for Tackling the Key Research, P. R. China (2019-WJ-11).

Notes and references

1 M. Richter, *Chem. Rev.*, 2004, **104**, 3003–3036.
2 W. Miao, *Chem. Rev.*, 2008, **108**, 2506–2553.
3 H. Qi and C. Zhang, *Anal. Chem.*, 2020, **92**, 524–534.
4 X. Ma, W. Gao, F. Du, F. Yuan, J. Yu, Y. Guan, N. Sojic and G. Xu, *Acc. Chem. Res.*, 2021, **54**, 2936–2945.
5 L. Li, Y. Chen and J. Zhu, *Anal. Chem.*, 2017, **89**, 358–371.
6 K. Muzyka, M. Saqib, Z. Liu, W. Zhang and G. Xu, *Biosens. Bioelectron.*, 2017, **92**, 241–258.
7 X. Huo, H. Lu, J. Xu, H. Zhou and H. Chen, *J. Mater. Chem. B*, 2019, **7**, 6469–6475.
8 E. Doeven, G. Barbante, C. Hogan and P. Francis, *Chempluschem*, 2015, **80**, 456–470.
9 B. Chang, K. Chow, J. Crooks, F. Mavre and R. Crooks, *Analyst*, 2012, **137**, 2827–2833.
10 W. Zhan, J. Alvarez and R. Crooks, *Anal. Chem.*, 2003, **75**, 313–318.
11 Y. Wang, R. Jin, N. Sojic, D. Jiang and H. Chen, *Angew. Chem., Int. Ed.*, 2020, **59**, 10416–10420.

12 A. Ismail, S. Voci, P. Pham, L. Leroy, A. Maziz, L. Descamps, A. Kuhn, P. Mailley, T. Livache, A. Buhot, T. Leichle, A. Bouchet-Spinelli and N. Sojic, *Anal. Chem.*, 2019, **91**, 8900–8907.
13 Z. Wei, A. Julio and M. Richard, *J. Am. Chem. Soc.*, 2002, **124**, 13265–13270.
14 N. Bell and U. Keyser, *J. Am. Chem. Soc.*, 2015, **137**, 2035–2041.
15 R. Yu, Y. Ying, Y. Hu, R. Gao and Y. Long, *Anal. Chem.*, 2017, **89**, 8203–8206.
16 K. Freedman, L. Otto, A. Ivanov, A. Barik, S. Oh and J. Edel, *Nat. Commun.*, 2016, **7**, 1–9.
17 R. Yu, Y. Ying, R. Gao and Y. Long, *Angew. Chem., Int. Ed.*, 2019, **58**, 3706–3714.
18 K. Xiao, L. Wen and L. Jiang, *Small*, 2016, **12**, 2810–2831.
19 T. Xiong, K. Zhang, Y. Jiang, P. Yu and L. Mao, *Sci. China: Chem.*, 2019, **62**, 1346–1359.
20 Y. Ying, J. Zhang, R. Gao and Y. Long, *Angew. Chem., Int. Ed.*, 2013, **52**, 13154–13161.
21 Z. Long, S. Zhan, P. Gao, Y. Wang, X. Lou and F. Xia, *Anal. Chem.*, 2018, **90**, 577–588.
22 Y. Lin, Y. Ying, R. Gao and Y. Long, *Chem. –Eur. J.*, 2018, **24**, 13064–13071.
23 Y. Jiang, N. Liu, W. Guo, F. Xia and L. Jiang, *J. Am. Chem. Soc.*, 2012, **134**, 15395–15401.
24 S. Cai, J. Sze, A. Ivanov and J. Edel, *Nat. Commun.*, 2019, **10**, 1–9.
25 W. Chang and J. Allen, *Anal. Chem.*, 1997, **69**, 4627–4633.
26 Y. Ma, J. Guo, L. Jia and Y. Xie, *ACS Sens.*, 2018, **3**, 167–173.
27 J. Cai, Q. He, L. Song, L. Han, B. Liu, Y. Zhao, W. Chen and D. Zhan, *J. Phys. Chem. C*, 2019, **123**, 26299–26308.
28 Y. Jiang, Y. Feng, J. Su, J. Nie, L. Cao, L. Mao, L. Jiang and W. Guo, *J. Am. Chem. Soc.*, 2017, **139**, 18739–18746.
29 P. Gao, Q. Ma, D. Ding, D. Wang, X. Lou, T. Zhai and F. Xia, *Nat. Commun.*, 2018, **9**, 1–11.
30 J. Liu, M. Kvetny, J. Feng, D. Wang, B. Wu, W. Brown and G. Wang, *Langmuir*, 2012, **28**, 1588–1595.
31 S. Li, D. Zhang, J. Liu, C. Cheng, L. Zhu, C. Li, Y. Lu, S. Low, B. Su and Q. Liu, *Biosens. Bioelectron.*, 2018, **129**, 284–291.
32 M. Wu, X. Sun, M. Zhu, H. Chen and J. Xu, *Chem. Commun.*, 2015, **51**, 14072–14075.
33 F. Yan, Y. He, L. Ding and B. Su, *Anal. Chem.*, 2015, **87**, 4436–4441.
34 X. Huang, X. Bian, L. Chen, L. Guo, B. Qiu and Z. Lin, *Anal. Chem.*, 2021, **93**, 10351–10357.
35 Y. Zhao, J. Yu, G. Xu, N. Sojic and G. Loget, *J. Am. Chem. Soc.*, 2019, **141**, 13013–13016.
36 X. Liu, L. Shi, W. Niu, H. Li and G. Xu, *Angew. Chem., Int. Ed.*, 2007, **119**, 425–428.
37 W. Lan, D. Holden and H. White, *J. Am. Chem. Soc.*, 2011, **133**, 13300–13303.
38 W. Lan, M. Edwards, L. Luo, R. Perera, X. Wu, C. Martin and H. White, *Acc. Chem. Res.*, 2016, **49**, 2605–2613.
39 Y. Youn, C. Lee, J. Kim, Y. Chang, D. Kim and K. Yoo, *Anal. Chem.*, 2016, **88**, 688–694.